HHS Public Access

Author manuscript

*Biochemistry*. Author manuscript; available in PMC 2016 June 13.

Published in final edited form as:

*Biochemistry*. 2013 December 3; 52(48): 8777–8785. doi:10.1021/bi401207q.

# The Cellular Environment Stabilizes Adenine Riboswitch RNA Structure

**Jillian Tyrrell**[†], **Jennifer L. McGinnis**[†], **Kevin M. Weeks**[†,*], and **Gary J. Pielak**[†,‡,§,*]

[†]Department of Chemistry, University of North Carolina at Chapel Hill, Chapel Hill, North Carolina 27599-3290, United States

[‡]Department of Biochemistry and Biophysics, University of North Carolina at Chapel Hill, Chapel Hill, North Carolina 27599-3290, United States

[§]Lineberger Comprehensive Cancer Center, University of North Carolina at Chapel Hill, Chapel Hill, North Carolina 27599-3290, United States

## Abstract

There are large differences between the intracellular environment and the conditions widely used to study RNA structure and function *in vitro*. To assess the effects of the crowded cellular environment on RNA, we examined the structure and ligand-binding function of the adenine riboswitch aptamer domain in healthy, growing *Escherichia coli* cells at single-nucleotide resolution on the minute timescale using SHAPE. The ligand-bound aptamer structure is essentially the same in cells and in buffer at 1 mM $Mg^{2+}$, the approximate $Mg^{2+}$ concentration we measured in cells. In contrast, the in-cell conformation of the ligand-free aptamer is much more similar to the fully folded ligand-bound state. Even adding high $Mg^{2+}$ concentrations to the buffer used for *in vitro* analyses did not yield the conformation observed for the free aptamer in cells. The cellular environment thus stabilizes the aptamer significantly more than does $Mg^{2+}$ alone. Our results show that the intracellular environment has a large effect on RNA structure that ultimately favors highly organized conformations.

## Abstract

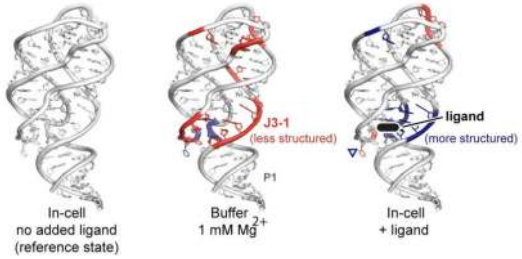


[*]**Corresponding Authors**: Gary J. Pielak, Genome Sciences 3250, University of North Carolina at Chapel Hill, Chapel Hill, NC 27699-3290, 919-966-3671, gary_pielak@unc.edu; Kevin M. Weeks, Genome Sciences 3258, University of North Carolina at Chapel Hill, Chapel Hill, NC 27699-3290, 919-962-7486, weeks@unc.edu.

Supporting Information

Supporting Figures S1-S11. This material is available free of charge via the Internet at http://pubs.acs.org.

The authors declare no competing financial interests.

**Keywords**

RNA; crowding; in-cell SHAPE; riboswitch

The intracellular environment is vastly different from the simple buffered solutions used in most *in vitro* explorations of biological macromolecular structure and function. For example, macromolecules reach concentrations of 300 g/L and occupy up to 30% of the total cellular volume[1] and cells contain complex mixtures of metabolites, ions, and polyamines.[2-4] The highly crowded intracellular environment increases the importance of two types of interactions between macromolecules: hard-core repulsions and chemical interactions.[5] Hard-core repulsions reflect the impenetrable nature of atoms. These interactions reduce the available conformational space, thus favoring compact states.[6, 7] Chemical interactions can be attractive or repulsive. Repulsions arise from contacts between like charges and reinforce the stabilizing hard-core effect. Attractive interactions include hydrogen-bonding, juxtaposed complementary charges, and hydrophobic contacts, and binding by numerous cellular proteins. Attractive interactions that expose more interacting surface to the crowding molecules destabilize folded, compact states,[8, 9] whereas specific protein binding will be stabilizing. Low molecular weight species in the cytoplasm including metabolites, polyamines and magnesium ion, also impose a combination of hard-core repulsions, non-specific chemical interactions, and direct binding that are difficult to recapitulate *in vitro.*

RNA molecules are responsible for diverse cellular functions, many governed by precise features of their three-dimensional structures. *In vitro* studies show that crowding by synthetic polymers has dramatic consequences on RNA folding.[10-12] In addition, the negatively charged backbone of RNA makes folding highly sensitive to cation and polyamine concentrations.[13, 14] Despite these considerations, most explorations of RNA structure and function employ purified RNAs and simple buffered solutions at $Mg^{2+}$ concentrations significantly higher than those in cells. Studies of RNA structure *in vitro* have yielded many important insights into the roles of structural motifs in RNA function; however, a critical goal is to quantitatively monitor and understand the structure of RNA and its interactions with small molecule and protein ligands in the cellular environment.

The most widely used approach to probe RNA structure in cells has employed the reagent dimethyl sulfate (DMS) and these studies have yielded important insights into the intracellular structure of several RNAs.[15, 16] However, DMS reacts with only a few functional groups, primarily adenosine (N1), to a lesser extent cytosine (N3), and with guanosine (N7, although this adduct is not generally assayed in *in vivo* studies). *In vivo* DMS probing studies are therefore best coupled with other information.[16]

Here, we apply SHAPE (selective 2′-hydroxyl acylation analyzed by primer extension) using the fast-acting 1M7 reagent, which reacts nearly equally with all four RNA nucleotides,[17] to probe the effect of the intracellular environment on RNA structure. SHAPE yields quantitative information on the degree to which a nucleotide is constrained by base pairing or other interactions and has been widely used to develop secondary structure models and to detect complex conformational changes in RNA *in vitro*[18-22], within membrane-encapsulated viruses[23, 24] and in cells.[25] Applying SHAPE chemistry to living cells

promises to improve our understanding of how the intracellular environment affects RNA structure.

Riboswitch RNAs regulate gene expression by undergoing ligand-induced conformational changes that ultimately enhance or inhibit expression of a linked gene.[26] The *add* adenine riboswitch structure has been well characterized *in vitro*. Its function *in vivo* depends on binding the small metabolite adenine with high specificity. In the absence of ligand, the aptamer domain has a disordered binding pocket; upon ligand binding, stable tertiary interactions form (Figure 1A).[26-31]

We probed the ligand-bound and ligand-free states of the adenine riboswitch aptamer domain in live *E. coli* cells. Although many non-specific RNA interactions occur in cells, adenine binding to the aptamer is highly specific and causes large and well defined changes SHAPE reactivity. The conformations of the ligand-bound aptamer in cells and in buffer were highly similar; in strong contrast, the ligand-free form was generally less reactive in cells than in buffer. Moreover, the pattern SHAPE reactivity in cells could not be achieved in buffers containing 30 times the intracellular $Mg^{2+}$ concentration. The results show that the net effect of the intracellular environment is to stabilize RNA tertiary structure, and emphasize the importance of studying and understanding RNA structure in cells.

## EXPERIMENTAL PROCEDURES

### Concentration of $Mg^{2+}$ in *E. coli* Cells

Free $Mg^{2+}$ was measured using the intracellular chelator, mag-fura-2, acetoxymethyl (AM). The free $Mg^{2+}$ concentration was obtained from the ratio of the fluorescence intensities of the free and complexed dyes at 510 nm measured using excitation 380 nm and 340 nm, respectively. Methods were adapted from those described previously.[33] *E. coli* BL21(DE3) cells were grown in LB at 37 °C, with shaking, until the optical density at 600 nm ($OD_{600}$) reached ~1. Aliquots (12 mL) were centrifuged at room temperature for 15 min at 1500 × *g*, washed once, and resuspended in 1.5 mL $Mg^{2+}$-free buffer [10 mM HEPES (pH 7.4), 200 mM potassium acetate, 5 mM NaCl]. Cells were incubated with shaking at 37 °C for 10 min, then 500 μl of dye mixture containing 20 μM mag-fura-2 AM and 60 μM Pluronic F-127 (Molecular Probes) was added. Dyes were prepared in $Mg^{2+}$-free buffer from mag-fura-2 AM (5 mM, in anhydrous DMSO) and Pluronic F-127 [20% (w/v) in DMSO] stocks. After dye addition, cells were incubated for 70 min at 37 °C with shaking. Cells were then washed, resuspended in 2 mL of $Mg^{2+}$-free buffer, and incubated for 30 min to ensure hydrolysis of the intracellular dye. Cells were then washed twice and resuspended in $Mg^{2+}$-free buffer to yield an $OD_{600}$ ~0.5 (~$2 \times 10^8$ cells/mL). Cell viability was determined by plating serial dilutions of cell suspensions on LB-agar plates containing 1 mg/mL ampicillin.

The fluorescence of cell suspensions (2.4 mL in a 3 mL cuvette with stirring) was measured at 37 °C using a Varian Cary Eclipse fluorimeter. Excitation at 340 nm and 380 nm was alternated at 1 s intervals, and emission was measured 510 nm. To quantify $Mg^{2+}$-dependent changes in fluorescence, $Mg^{2+}$ was added to cells at 100 s intervals (Figure S1A of Supporting Information). The intensities and 340 nm/380 nm ratios were used to calculate the internal $Mg^{2+}$ concentration:[34]

$$\left[Mg^{2+}\right] = K_D\,(F_0/F_S)\,(R - R_{min})\,/\,(R_{max} - R) \quad (1)$$

where $K_D$ is the dissociation constant of the mag-fura-2/$Mg^{2+}$ complex (2.5 mM, see below), $F_0/F_S$ is the ratio of intensities with 380 nm excitation for no added $Mg^{2+}$ and saturating $Mg^{2+}$, R is the ratio of 510 nm emission from excitation at 340 nm and 380 nm at a given external $Mg^{2+}$ concentration, and $R_{min}$ and $R_{max}$ are the minimum and maximum ratios determined at 0 mM and saturating $Mg^{2+}$, respectively. $R_{min}$ and $R_{max}$ were obtained at the end of each experiment by adding $Mg^{2+}$ to a final concentration of 30 mM, then adding SDS [to 0.1% (w/v) final] to lyse the cells; lysis causes mag-fura-2 to be released from cells and to be saturated with extracellular $Mg^{2+}$ (Figure S1B of Supporting Information). This step was followed by addition of EDTA to a final concentration of 60 mM to chelate $Mg^{2+}$ and achieve a free $Mg^{2+}$ measurement. The $K_D$ was determined by recording $Mg^{2+}$-dependent fluorescence changes for hydrolyzed mag-fura-2 (0.4 μM) in buffer and fitting the 510 nm intensities from 340 nm excitation to a one-site binding curve (Figure S2 of Supporting Information). Emission from cells in $Mg^{2+}$-free buffer was constant over time (Figure S1A of Supporting Information). Intensities were corrected for autofluorescence, which was also constant and lower than that of dye-loaded cells by a factor of 13 for excitation at 340 nm and a factor of 20 for excitation at 380 nm (Inset to Figure S1B of Supporting Information). Serial dilution and plating of cells confirmed that ~90% of the dye-loaded cells were viable.

## Vector Construction

The sequence encoding the adenine riboswitch aptamer domain was inserted between the TΨC and D stem-loops of human $tRNA^{lys3}$ as a synthetic gene in a pIDTSMART vector (IDT) (Figure S3 of Supporting Information). The gene was inserted into pET21a(+) using *Hind* III (5′) and *Xba* I (3′) cloning sites for expression under the control of a T7 promoter (Figure S3 of Supporting Information). The transcript is a chimeric tRNA in which the anti-codon stem is replaced by the adenine riboswitch aptamer domain.[35, 36]

## RNA Expression

The aptamer-tRNA construct (Figure 1B) was expressed in BL21(DE3) *E. coli* cells in LB medium at 37 °C. When the $OD_{600}$ reached 0.6, RNA expression was induced by addition of isopropyl-β-D-1-thiogalactopyranoside (1 mM). Expression was allowed to proceed for 30 min, at which time aliquots were removed and added to 2-aminopurine, 2,6-diaminopurine, or 3-methyladenine dissolved in LB (final concentration 1 mM) or to LB alone. Expression was continued for 1 h, at which time cell aliquots were subjected to either in-cell or *in vitro* SHAPE.

## In-Cell SHAPE

The aptamer construct was expressed in the presence or absence of ligand as described above. Following RNA expression, cellular RNA was modified by adding aliquots of cells (1 mL) to 20 μL of 300 mM 1M7 in DMSO or to neat DMSO (2% vol/vol final co-solvent).

The samples were incubated with shaking for 3 min at 37 °C. Total cellular RNA was recovered from protoplasts and isolated as described.[37] RNA was precipitated with ethanol, washed three times with 70% (vol/vol) aqueous ethanol, and resuspended in 15 μL of deionized $H_2O$. Primer extension of the aptamer construct was achieved using sequence-specific primers, containing locked nucleic acid (LNA) nucleotides, and 5' fluorescent labels as outlined below. cDNA products were resolved by capillary electrophoresis.

To measure the concentration of aptamer construct in the cellular RNA, aliquots of total RNA and serial dilutions of purified construct were analyzed by denaturing polyacrylamide gel electrophoresis. Gels were stained with SYBR Gold (Invitrogen) and a standard curve was constructed using the band intensities of samples corresponding to the purified construct. The standard curve was used to determine the concentration of the aptamer construct in the total RNA samples. The aptamer construct (~7 g/L) was ~7% of the total RNA concentration (100 g/L determined by UV spectroscopy). We estimated the concentration of the aptamer construct in cells as 7% to the total RNA in *E. coli* (75-120 g/L[38]). From the molecular weight of the construct (43.4 kD), the concentration of construct in cells is 120-190 μM.

### *In Vitro* SHAPE

Following expression, RNA was recovered from protoplasts and isolated as described[37] and incubated in 50 mM HEPES (pH 8.0), 200 mM potassium acetate (pH 8.0) and 1 to 30 mM $MgCl_2$ for 30 min. The aptamer construct was purified by anion exchange, fast performance liquid chromatography. Ligand (1 mM) was added after folding and incubation was continued for 10 min. The aptamer construct (8 pmol) was then added to 1/50 volume 300 mM 1M7 in DMSO or to neat DMSO. The samples were incubated at 37 °C for 3 min. RNA was precipitated with ethanol, washed three times with 70% (vol/vol) aqueous ethanol, and resuspended in 15 μL deionized $H_2O$.[37] Primer extension and capillary electrophoresis were then used to determine sites of adduct formation.

### Primer extension

A 12-nt DNA primer (Exiqon) complementary to the 5′ end of the acceptor stem and containing three locked nucleic acid (LNA) nucleotides (5′-*T*G*G*C*G*CCCGAAC-3′; italic font indicates LNA nucleotides) was used. The primer was labeled with either a 5′ 6-FAM or 5-HEX fluorescent dye. The 6-FAM labeled primer was used for the (+) or (−) 1M7 channels; the 5-HEX was used for the sequencing channel. RNA (1.5 μg) and primer (2 pmol) were mixed and diluted to 13 μL with $H_2O$. The sample was then incubated for 5 min at 65 °C and then on ice for 3 min. The reaction mixture contained 4 μL of 5× SuperScript first-strand buffer, 1 μL 0.1 M dithiothreitol, 1 μL dNTPs (10 mM each), and 1 U SuperScript III (Invitrogen). For sequence analysis, the reactions were prepared as described above, except the RNA was not treated with 1M7 or DMSO, the RNA-primer mixture was diluted to 12 μL, and 1 μL of 10 mM ddATP was added prior to adding SuperScript III. Reactions were incubated at 55 °C for 60 min, and then at 70 °C for 15 min. cDNA was recovered by ethanol precipitation and washed three times with 70% (vol/vol) aqueous ethanol. Pellets were dried under vacuum and resuspended in 10 μL of deionized formamide.

The products were resolved by capillary electrophoresis on an Applied Biosystems 3500 DNA capillary electrophoresis instrument.

### SHAPE Data Analysis

Electropherograms were analyzed with QuShape.[39] After baseline and mobility shift corrections, peaks in the (+) and (−) 1M7 channels were aligned, and Gaussian integration was used to quantify peaks areas. The SHAPE reactivity is reported as the area of the (+) 1M7 peaks minus the area of the no-reagent background peaks. The absolute amount of adduct formation *in vitro* and in cells was calculated based on the probabilities of termination of primer extension, as described.[39]

## RESULTS

### Intracellular $Mg^{2+}$ Concentration

RNA tertiary structure depends on the $Mg^{2+}$ concentration.[13, 31] We measured the free $Mg^{2+}$ concentration in *E. coli* cells using a ratiometric $Mg^{2+}$-selective fluorophore (Figure 2, Figures S1 and S2 of Supporting Information)[34] to ensure that relevant concentrations were used for *in vitro* experiments. Cells were grown to late-log phase, and the intracellular $Mg^{2+}$ concentration was quantified as a function of external $Mg^{2+}$ concentration. At an external concentration corresponding to that in LB medium (0.3 mM, calculated from the $Mg^{2+}$ content of Tryptone and yeast extract[40]), the intracellular $Mg^{2+}$ concentration was 0.8 ± 0.2 mM (Figure 2, arrow). The intracellular free $Mg^{2+}$ concentration increased only slightly with increasing extracellular concentration; the concentration did not rise above 1 mM until the extracellular concentration was 5 mM and reached 2.2 ± 0.5 mM at an external concentration of 10 mM (Figure 2). Our measurement of the free $Mg^{2+}$ concentration in *E. coli* cells (0.8 ± 0.2 mM) is consistent with measurements of free $Mg^{2+}$ in other cell types.[41-43, 33]

### In-Cell SHAPE

To study the aptamer domain in *E. coli* cells, we expressed the RNA as a chimera in which the aptamer domain was inserted into the anticodon loop of $tRNA^{lys}$ (Figure 1A and Figure S3 of Supporting Information). These chimeric RNAs fold stably in cells and are processed by nucleases that cleave tRNAs to yield an intact and monodisperse product.[35, 36] The RNA containing the aptamer was processed into a product of approximately 143 nucleotides (Figure 1B).

In-cell SHAPE probing was achieved by adding 1-methyl-7-nitroisatoic anhydride (1M7)[44] in dimethyl sulfoxide (DMSO) to late log-phase cells, under conditions compatible with normal cell growth and viability (Figure S4 of Supporting Information). 1M7 has a half-life of 24 s under conditions corresponding to those in culture media at late log phase (37 °C and pH 7.0, Figure S5 of Supporting Information). A wide variety of experiments, spanning roughly 30 years of experimental work, suggest that small, slightly hydrophobic molecules penetrate cellular membranes and diffuse over the dimensions of an *E. coli* bacterium on a timescale of roughly 30-100 ms.[45-47, 23, 24, 48, 49] Thus, the half-life of 1M7 is roughly 1000-

times longer than the time required to diffuse the length of an *E. coli* cell. In-cell RNA probing with 1M7 yields structural snapshots on the minute timescale.

We have consistently found that 1M7 is straightforward to use in cells, including bacterial cells. Reagents like 1M7 that react rapidly with RNA and reagents that react slowly[25] probe different structural features. In general, reagents that react on the minute timescale provide quantitative measurements of intrinsic RNA structure,[50-52] whereas slower reagents are sensitive to additional slower dynamic features of RNA, some of which vary with the ion environment. One consequence of this difference is that slow reagents are highly sensitive to *in vitro* ion concentrations,[44] whereas fast reagents are not. Thus, fast-reacting reagents like 1M7 are to be strongly preferred for making direct comparisons of in-cell and *in vitro* measurements without need for corrections based on ion sensitivity.

After modification with 1M7, total cellular RNA was isolated, and sites of aptamer modification were detected by primer extension analyzed by capillary electrophoresis.[37] In-cell SHAPE probing with 1M7 yielded electropherograms comparable or better in quality to those obtained from *in vitro* experiments (Figures 3A and 3B). SHAPE reactivities were highly reproducible for both *in vitro* and in-cell experiments (Figure S6 of Supporting Information). Little or no degradation of the adenine riboswitch RNA was observed in the cells or *in vitro* upon treatment with DMSO. We also calculated the absolute amount of adduct formation for the free RNA, both in dilute solution and in cells, by integrating all observed peaks and calculating the amount of unmodified, full-length product.[39] The numbers of adducts per RNA were identical at 0.60 and 0.61, respectively. This corresponds to one modification every ~105 nucleotides both *in vitro* and in cells, or roughly one adduct per RNA. Thus, signals reflected reactivity of the RNA with 1M7 and, as expected,[45-47, 23, 24, 48, 49] the 1M7 reagent readily diffuses across the double walled membrane of the Gram-negative *E. coli* bacterium.

In the in-cell reactivity profile for the aptamer in the absence of added ligand (Figure 3C and Figure S6 of Supporting Information), nucleotides expected to form helices P1, P2, and P3 (Figure 1A) had low reactivity, consistent with stable base pairing in these structures. Most nucleotides that form the ligand binding pocket (J1-2, J2-3, J3-1) were moderately ( ≥0.4) or highly (>0.8) reactive as were nucleotides in the loop regions L2 and L3. Nucleotide U48 was hyper-reactive. The in-cell SHAPE reactivity profile for the free aptamer suggests the three major RNA helices are formed and that the ligand-binding pocket is flexible and partially disordered.

## The Ligand-Free RNA Is More Highly Organized in Cells Than in Buffered Solution

We observed large differences between the structure of the unliganded aptamer in cells and its structure in buffer at 1 mM $Mg^{2+}$ (Figure 3C). We subtracted the two SHAPE profiles from each other and identified statistically significant nucleotide reactivity differences (two-tailed Students t-test; $p < 0.02$, n=3) (Figure 3D). Nucleotides G37 and G38 in L2 and C61 and C62 in L3 were significantly more reactive *in vitro* than in cells, suggesting that tertiary interactions involving loops L2 and L3[32, 31] were largely absent in buffered solution but were at least partially formed in cells.

Most nucleotides in the adenine binding pocket (regions J2-3 and J3-1) were also less reactive in cells than *in vitro*, consistent with formation of stacking and base pairing interactions in these regions in cells and the lack of these interactions in buffer. The major exceptions were two nucleotides in J1-2, which were more reactive in cells than in buffered solution. This higher reactivity may arise from increased solvent accessibility due to tertiary collapse and ordering of J2-3 and J3-1 or to attractive chemical interactions with other cellular components. Nucleotide U48 was hyper-reactive in cells but only highly reactive in buffer. In the crystal structure of the ligand-bound RNA, U48 is flipped into the solvent[32] and constrained in one of the rare conformations that activates the ribose 2′-hydroxyl group for SHAPE chemistry (Figure S7 of Supporting Information).[53] Thus, hyper-reactivity at U48 is also indicative of a more highly structured RNA in cells.

Overall, as judged by nucleotide reactivities that report the L2-L3 tertiary interaction and the organization of the ligand-binding pocket, the aptamer features more nucleotides whose conformations are similar to the fully folded ligand bound state, suggesting it is more structured and has a more highly organized binding pocket in cells than in buffer at a physiological $Mg^{2+}$ concentration.

## Ligand Binding in Cells

The *add* riboswitch recognizes 2-aminopurine (2AP) (Figure 4A) and adenine with similar affinities ($K_d$ ~117 nM and 60 nM, respectively[27, 54, 55]), and both ligands induce large conformational changes in the riboswitch RNA.[26, 54, 55] 2AP, however, is not found in detectable quantities in *E. coli*, and the expression level of our RNA construct is ~100 times the intracellular concentration of adenine (~$10^{-6}$ M).[4] Thus, using 2AP, it is possible to examine the in-cell consequences of ligand binding without interference by endogenous cellular metabolites.

We observed numerous changes in SHAPE reactivity for the aptamer expressed in *E. coli* when 2AP was added to the growth medium (Figure 4A). Significant differences (two-tailed Students t-test; $p < 0.02$, $n = 3$) are consistent with ligand-mediated conformational changes in the RNA and formation of the intricate network of base-pairing and stacking interactions observed both crystallographically[32] and by NMR[30] (Figure 4C, black bars). Specifically, reactivities in the binding pocket decreased (Figure 4A, regions J1-2 and J3-1), whereas reactivities increased at U62 and U63, consistent with the crystal structure that shows that these nucleotides are unpaired and likely highly dynamic in the ligand-bound state.[32] The reactivity of U48 increased two-fold upon addition of 2AP (Figure 4A; $p < 0.04$, also consistent with the crystal structure of the ligand-bound RNA, which shows that this position is constrained in a conformation that facilitates SHAPE reactivity (Figure S7 of Supporting Information).[32, 53]

Addition of 2AP to the aptamer *in vitro* also induced large conformational changes in the RNA (Figures 4B and 4C). The SHAPE profiles of the ligand-bound RNA in cells and in buffer with $Mg^{2+}$ were similar (Figure S8 of Supporting Information; also compare Figures 4A and 4B). Because the starting structures of the RNA in cells and in buffer are different, the degree of conformational change induced by ligand binding in cells is different (and generally smaller than) than the ligand-induced change in buffer (Figure 4C). In cells, there

were only small changes in regions L2, J2-3, and J3-1 upon ligand binding. In buffer, the aptamer underwent substantial reactivity changes in these regions. In contrast, conformations of nucleotides in regions J1-2 and L3 changed more dramatically upon ligand binding in cells than in buffer. Overall, these observations indicate that the equilibrium between the free and bound aptamer states is different, and likely more favorable, in cells than in buffer.

We assessed the specificity of the conformational changes induced by 2AP with two additional ligands. 2,6-Diaminopurine binds the aptamer with high affinity ($K_D \approx 2$ nM).[55] As expected, this ligand also induced large changes in the in-cell aptamer SHAPE reactivity profile, and these changes were comparable to those induced by 2AP (Figure S9 of Supporting Information). In contrast, *N*6, *N*6-dimethyl-adenine does not bind the aptamer ($K_D > 300$ μM),[26] and the in-cell SHAPE profile obtained from cells grown in the presence of this molecule was similar to that of the free aptamer (Figure S9 of Supporting Information). These results emphasize that conformational changes induced by 2AP reflect specific binding in the ligand-binding pocket of the riboswitch.

## Differences Between In-Cell and Dilute Solution Structures Reflect Intrinsic Properties of the Riboswitch RNA

To confirm that differences between in-cell and *in vitro* SHAPE reactivity profiles of the free aptamer were not due to binding by endogenous adenine, we investigated a non-binding mutant of the aptamer. U74 forms a canonical base pair with the adenine ligand that is critical for both ligand affinity and specificity.[26, 54] We reasoned that a U74G mutation should disrupt binding to adenine, 2AP, and related molecules. The profiles of the U74G mutant in buffer at 1 mM $Mg^{2+}$ in the absence and presence of 1 mM 2AP were essentially identical (Figure S10 of Supporting Information), indicating that the mutant does not bind 2AP *in vitro*, even at high ligand concentrations.

In-cell analysis of the U74G mutant in the absence and presence of added 2AP also yielded nearly identical profiles (Figure 5A), indicating that the mutant does not bind ligand in cells. Critically, the non-binding mutant exhibits differences between in-cell and *in vitro* states similar to those observed for the native sequence aptamer (Figures 5B and 5C). Thus, the non-binding mutant and the native sequence aptamer adopt the same organized structure in cells, even in the absence of ligand. Therefore, the in-cell structure of the unliganded native sequence aptamer does not reflect binding by endogenous adenine. Instead, these data emphasize a critical role for the intracellular environment in governing the structure of this RNA.

## High $Mg^{2+}$ Concentrations Do Not Induce the Structure Observed In Cells

We attempted to induce the aptamer domain to adopt the in-cell conformation *in vitro* by increasing the added $Mg^{2+}$ concentration. We probed the aptamer structure as a function of $Mg^{2+}$ concentration and calculated the Pearson correlation coefficient ($R$) between in-cell and *in vitro* SHAPE reactivities (Figure 6). The correlation between the in-cell reactivities and those measured in buffer at 1 mM $Mg^{2+}$ was low (0.55, inset in Figure 6), consistent with large differences in RNA structure under these two conditions. At a $Mg^{2+}$ concentration

of 2 mM, the coefficient was 0.69. At 5 mM, the coefficient was 0.75, and no additional increase was observed up to the highest concentration tested, 30 mM $Mg^{2+}$. These data emphasize that, even in the presence of high $Mg^{2+}$ concentrations, the ligand-free aptamer structure *in vitro* is different from that observed in cells. In summary, the conformation of the free aptamer RNA in cells features significantly more nucleotides whose conformations are similar to the fully folded ligand-bound state than to the structure that predominates under typical dilute solution conditions. Importantly, the in-cell state cannot be recapitulated in buffer by addition of a high concentration of $Mg^{2+}$ ion.

## DISCUSSION

The adenine riboswitch controls expression of an adenosine deaminase gene in response to adenine levels. Like many non-coding RNAs, riboswitch function is mediated by the higher-order structure of the RNA. The crowded and unique ion environment in cells is likely to have a strong impact on RNA structure-function relationships, but these effects remain largely unexplored. We probed the reactivities of individual nucleotides in the aptamer RNA with the SHAPE reagent, 1M7, which readily diffuses through the *E. coli* bacterium, modifies RNA *in vitro* and in cells with roughly equal probability, and measures RNA structure on the timescale of minutes. We found that the cellular environment induces a conformation in the unbound adenine riboswitch aptamer RNA that is different from both the unliganded structure *in vitro*, even in buffer at high $Mg^{2+}$ concentrations, and from the ligand-bound structure.

We visualized differences between structures of the adenine riboswitch aptamer domain in cells with other states examined here by superimposing statistically significant reactivity differences on the structure of the fully folded, ligand-bound RNA. For the in-cell, ligand-free RNA (Figure 7, left-most structure), SHAPE reactivities suggest that long-range interactions between L2 and L3 are partially formed but that the J1-2 and J3-1 strands in the ligand-binding pocket are relatively unstructured (compare Figures 7A and 7C). In buffer at 1 mM $Mg^{2+}$, nucleotides throughout the aptamer domain, including those in both the binding pocket and loop regions, are more reactive by SHAPE than in cells (Figure 7B, red regions). Nucleotides that form the L2-L3 tertiary interaction stabilize a collapsed form of the adenine aptamer that reduces the radius of gyration of the RNA by ~3 Å.[31] These data indicate that the RNA in healthy living cells is less reactive, likely more compact, and more highly structured than the purified RNA in buffer at 1 mM $Mg^{2+}$ (Figures 7A and 7B).

In cells, the non-binding U74G mutant has SHAPE reactivities virtually identical to those of the ligand-free, native sequence aptamer (Figure 5), emphasizing that the decrease in reactivity in cells does not arise from endogenous ligand binding. Addition of 2AP to the native sequence RNA in cells induced changes in SHAPE reactivity that fell largely in binding pocket (J1-2 and J3-1) regions (Figure 7C). The localized changes that differentiate the in-cell and plus-ligand states emphasize that much of the global RNA structure is at least partially stable in cells and that effects due to 2AP binding occur predominately in the ligand-binding pocket (compare Figures 7A and 7C).

Strikingly, in buffer at 30 mM $Mg^{2+}$, SHAPE reactivities indicate that the aptamer domain structure is more similar to the structure in 1 mM $Mg^{2+}$ than to the in-cell state (Figure 7D). Therefore, the cellular environment stabilizes the ligand-free aptamer to yield a higher-order structure that is not replicated by ligand binding or by high $Mg^{2+}$ concentrations *in vitro*.

In summary, we examined the structure of the adenine riboswitch aptamer RNA in living cells at single-nucleotide resolution on the minute timescale using the fast-acting 1M7 SHAPE reagent.[44, 50, 53, 52] The intracellular environment induces a less SHAPE-reactive (and thus more highly conformationally constrained) conformation in the ligand-free aptamer, indicating that the unliganded RNA is significantly less structured *in vitro* than in cells. Widely used standard *in vitro* conditions, even at high $Mg^{2+}$ concentrations, do not recapitulate the aptamer structure in cells. The complex cellular environment contains diverse small and large molecules that impose a combination hard-core repulsions and repulsive and attractive chemical interactions on RNA.[9] Our observation that, in cells, the aptamer RNA is characterized by significantly more nucleotides whose conformations are similar to the fully folded ligand-bound state suggests that, overall, the in-cell environment exerts a strong net stabilizing effect on RNA structure. These differences in levels of RNA organization, readily detectable by SHAPE in-cell probing, are likely to have wide ranging consequences for RNA structure and function.

## Supplementary Material

Refer to Web version on PubMed Central for supplementary material.

## Acknowledgments

We thank Luc Ponchon for guidance with the tRNA scaffold expression system; Oleg Favorov and Fethullah Karabiber for assistance with calculating the absolute amount of adduct formation *in vitro* and in cells; and Linda Spremulli for insightful discussions.

**Funding**

This work was supported by grants from the National Science Foundation, MCB-1051819 (to G.J.P.) and MCB-1121024 (to K.M.W.), and a National Science Foundation Graduate Research Fellowship (DGE-0646083 to J.T.).

## REFERENCES

(1). Zimmerman SB, Trach SO. Estimation of macromolecule concentrations and excluded volume effects for the cytoplasm of *Escherichia coli*. J. Mol. Biol. 1991; 222:599–620. [PubMed: 1748995]

(2). Tabor CW, Tabor H. Polyamines in microorganisms. Microbiol. Rev. 1985; 49:81–99. [PubMed: 3157043]

(3). Miyamoto S, Kashiwagi K, Ito K, Watanabe S, Igarashi K. Estimation of polyamine distribution and polyamine stimulation of protein synthesis in *Escherichia coli*. Arch. Biochem. Biophys. 1993; 300:63–68. [PubMed: 7678729]

(4). Bennett BD, Kimball EH, Gao M, Osterhout R, Van Dien SJ, Rabinowitz JD. Absolute metabolite concentrations and implied enzyme active site occupancy in *Escherichia coli*. Nat. Chem. Biol. 2009; 5:593–599. [PubMed: 19561621]

(5). Wang Y, Sarkar M, Smith AE, Krois AS, Pielak GJ. Macromolecular crowding and protein stability. J. Am. Chem. Soc. 2012; 134:16614–16618. [PubMed: 22954326]

(6). Minton AP. Excluded volume as a determinant of macromolecular structure and reactivity. Biopolymers. 1981; 20:2093–2120.

(7). Zhou HX, Rivas G, Minton AP. Macromolecular crowding and confinement: biochemical, biophysical, and potential physiological consequences. Annu. Rev. Biophys. 2008; 37:375–397. [PubMed: 18573087]

(8). Sarkar M, Smith AE, Pielak GJ. Impact of reconstituted cytosol on protein stability. Proc. Natl. Acad. Sci. U.S.A. 2013 in press.

(9). Sarkar M, L. C, Pielak GJ. Soft interactions and crowding. Biophys. Rev. 2013; 5:187–194.

(10). Nakano S, Karimata HT, Kitagawa Y, Sugimoto N. Facilitation of RNA enzyme activity in the molecular crowding media of cosolutes. J. Am. Chem. Soc. 2009; 131:16881–16888. [PubMed: 19874030]

(11). Denesyuk NA, Thirumalai D. Crowding promotes the switch from hairpin to pseudoknot conformation in human telomerase RNA. J. Am. Chem. Soc. 2011; 133:11858–11861. [PubMed: 21736319]

(12). Kilburn D, Roh JH, Guo L, Briber RM, Woodson SA. Molecular crowding stabilizes folded RNA structure by the excluded volume effect. J. Am. Chem. Soc. 2011; 132:8690–8696. [PubMed: 20521820]

(13). Draper DE. A guide to ions and RNA structure. RNA. 2004; 10:335–343. [PubMed: 14970378]

(14). Trachman RJ 3rd, Draper DE. Comparison of interactions of diamine and $Mg^{2+}$ with RNA rertiary structures: Similar versus differential effects on the stabilities of diverse RNA folds. Biochemistry. 2013; 52:5911–5919. [PubMed: 23899366]

(15). Wells SE, Hughes JM, Igel AH, Ares M Jr. Use of dimethyl sulfate to probe RNA structure *in vivo*. Meth. Enzymol. 2000; 318:479–493. [PubMed: 10890007]

(16). Liebeg A, Waldsich C. Probing RNA structure within living cells. Meth. Enzymol. 2009; 468:219–238. [PubMed: 20946772]

(17). Wilkinson KA, Vasa SM, Deigan KE, Mortimer SA, Giddings MC, Weeks KM. Influence of nucleotide identity on ribose 2′-hydroxyl reactivity in RNA. RNA. 2009; 15:1314–1321. [PubMed: 19458034]

(18). Merino EJ, Wilkinson KA, Coughlan JL, Weeks KM. RNA structure analysis at single nucleotide resolution by selective 2′-hydroxyl acylation and primer extension (SHAPE). J. Am. Chem. Soc. 2005; 127:4223–4231. [PubMed: 15783204]

(19). Wang B, Wilkinson KA, Weeks KM. Complex ligand-induced conformational changes in tRNA(Asp) revealed by single-nucleotide resolution SHAPE chemistry. Biochemistry. 2008; 47:3454–3461. [PubMed: 18290632]

(20). Weeks KM, Mauger DM. Exploring RNA structural codes with SHAPE chemistry. Acc. Chem. Res. 2011; 44:1280–1291. [PubMed: 21615079]

(21). Grohman JK, Gorelick RJ, Lickwar CR, Lieb JD, Bower BD, Znosko BM, Weeks KM. A guanosine-centric mechanism for RNA chaperone function. Science. 2013; 340:190–195. [PubMed: 23470731]

(22). Hajdin CE, Bellaousov S, Huggins W, Leonard CW, Mathews DH, Weeks KM. Accurate SHAPE-directed RNA secondary structure modeling, including pseudoknots. Proc. Natl. Acad. Sci. U.S.A. 2013; 110:5498–5503. [PubMed: 23503844]

(23). Wilkinson KA, Gorelick RJ, Vasa SM, Guex N, Rein A, Mathews DH, Giddings MC, Weeks KM. High-Throughput SHAPE analysis reveals structures in HIV-1 genomic RNA strongly conserved across distinct biological states. PLoS Biol. 2008; 6:e96. [PubMed: 18447581]

(24). Gherghe C, Lombo T, Leonard CW, Datta SAK, Bess JW, Gorelick RJ, Rein A, Weeks KM. Definition of a high-affinity Gag recognition structure mediating packaging of a retroviral RNA genome. Proc. Natl. Acad. Sci. U.S.A. 2010; 107:19248–19253. [PubMed: 20974908]

(25). Spitale RC, Crisalli P, Flynn RA, Torre EA, Kool ET, Chang HY. RNA SHAPE analysis in living cells. Nat. Chem. Biol. 2013; 9:18–20. [PubMed: 23178934]

(26). Mandal M, Breaker RR. Gene regulation by riboswitches. Nat. Rev. Mol. Cell. Biol. 2004; 5:451–463. [PubMed: 15173824]

(27). Lemay JF, Penedo JC, Tremblay R, Lilley DM, Lafontaine DA. Folding of the adenine riboswitch. Chem. Biol. 2006; 13:857–868. [PubMed: 16931335]

(28). Rieder R, Lang K, Graber D, Micura R. Ligand-induced folding of the adenosine deaminase A-riboswitch and implications on riboswitch translational control. ChemBioChem. 2007; 8:896–902. [PubMed: 17440909]

(29). Lin JC, Thirumalai D. Relative stability of helices determines the folding landscape of adenine riboswitch aptamers. J. Am. Chem. Soc. 2008; 130:14080–14081. [PubMed: 18828635]

(30). Lee MK, Gal M, Frydman L, Varani G. Real-time multidimensional NMR follows RNA folding with second resolution. Proc. Natl. Acad. Sci. U.S.A. 2010; 107:9192–9197. [PubMed: 20439766]

(31). Leipply D, Draper DE. Effects of $Mg^{2+}$ on the free energy landscape for folding a purine riboswitch RNA. Biochemistry. 2011; 50:2790–2799. [PubMed: 21361309]

(32). Serganov A, Yuan YR, Pikovskaya O, Polonskaia A, Malinina L, Phan AT, Hobartner C, Micura R, Breaker RR, Patel DJ. Structural basis for discriminative regulation of gene expression by adenine- and guanine-sensing mRNAs. Chem. Biol. 2004; 11:1729–1741. [PubMed: 15610857]

(33). Froschauer EM, Kolisek M, Dieterich F, Schweigel M, Schweyen RJ. Fluorescence measurements of free [$Mg^{2+}$] by use of mag-fura 2 in *Salmonella enterica*. FEMS Microbiol. Lett. 2004; 237:49–55. [PubMed: 15268937]

(34). Grynkiewicz G, Poenie M, Tsien RY. A new generation of $Ca^{2+}$ indicators with greatly improved fluorescence properties. J. Biol. Chem. 1985; 260:3440–3450. [PubMed: 3838314]

(35). Ponchon L, Dardel F. Recombinant RNA technology: The tRNA scaffold. Nat. Methods. 2007; 4:571–576. [PubMed: 17558412]

(36). Ponchon L, Beauvais G, Nonin-Lecomte S, Dardel F. A generic protocol for the expression and purification of recombinant RNA in *Escherichia coli* using a tRNA scaffold. Nat. Protoc. 2009; 4:947–959. [PubMed: 19478810]

(37). Deigan KE, Li TW, Mathews DH, Weeks KM. Accurate SHAPE-directed RNA structure determination. Proc. Natl. Acad. Sci. U.S.A. 2009; 106:97–102. [PubMed: 19109441]

(38). Cayley S, Lewis BA, Guttman HJ, Record MT Jr. Characterization of the cytoplasm of *Escherichia coli* K-12 as a function of external osmolarity. Implications for protein-DNA interactions *in vivo*. J. Mol. Biol. 1991; 222:281–300. [PubMed: 1960728]

(39). Karabiber F, McGinnis JL, Favorov OV, Weeks KM. QuShape: Rapid, accurate, and best-practices quantification of nucleic acid probing information, resolved by capillary electrophoresis. RNA. 2013; 19:63–73. [PubMed: 23188808]

(40). Sechan Wee BJW. Insights into the cell envelope of *Paracoccus denitrificans*, a member of the α-subdivision of purple bacteria, through studies of its lysozyme susceptibility. Can. J. Microbiol. 1988; 34:952–959.

(41). London RE. Methods for measurement of intracellular magnesium: NMR and fluorescence. Annu. Rev. Physiol. 1991; 53:241–258. [PubMed: 2042961]

(42). Hurley TW, Ryan MP, Brinck RW. Changes of cytosolic $Ca^{2+}$ interfere with measurements of cytosolic $Mg^{2+}$ using mag-fura-2. Am. J. Physiol. 1992; 263:C300–307. [PubMed: 1514577]

(43). Tashiro M, Konishi M. Basal intracellular free $Mg^{2+}$ concentration in smooth muscle cells of guinea pig tenia cecum: intracellular calibration of the fluorescent indicator furaptra. Biophys. J. 1997; 73:3358–3370. [PubMed: 9414246]

(44). Mortimer SA, Weeks KM. A fast-acting reagent for accurate analysis of RNA secondary and tertiary structure by SHAPE chemistry. J. Am. Chem. Soc. 2007; 129:4144–4145. [PubMed: 17367143]

(45). Mastro AM, Babich MA, Taylor WD, Keith AD. Diffusion of a small molecule in the cytoplasm of mammalian cells. Proc. Natl. Acad. Sci. U.S.A. 1984; 81:3414–3418. [PubMed: 6328515]

(46). Safranyos RG, Caveney S. Rates of diffusion of fluorescent molecules via cell-to-cell membrane channels in a developing tissue. J. Cell Biol. 1985; 100:736–747. [PubMed: 3972892]

(47). Jasnin M, Moulin M, Haertlein M, Zaccai G, Tehei M. Down to atomic-scale intracellular water dynamics. EMBO Rep. 2008; 9:543–547. [PubMed: 18451876]

(48). Mika JT, Van Den Bogaart G, Veenhoff L, Krasnikov V, Poolman B. Molecular sieving properties of the cytoplasm of *Escherichia coli* and consequences of osmotic stress. Mol. Microbiol. 2010; 77:200–207. [PubMed: 20487282]

(49). Mika JT, Poolman B. Macromolecule diffusion and confinement in prokaryotic cells. Curr. Opin. Biotechnol. 2011; 22:117–126. [PubMed: 20952181]

(50). Gherghe CM, Mortimer SA, Krahn JM, Thompson NL, Weeks KM. Slow conformational dynamics at C2′-endo nucleotides in RNA. J. Am. Chem. Soc. 2008; 130:8884–8885. [PubMed: 18558680]

(51). Mortimer SA, Weeks KM. C2′-endo nucleotides as molecular timers suggested by the folding of an RNA domain. Proc. Natl. Acad. Sci. U.S.A. 2009; 106:15622–15627. [PubMed: 19717440]

(52). Steen KA, Rice GM, Weeks KM. Fingerprinting noncanonical and tertiary RNA structures by differential SHAPE reactivity. J. Am. Chem. Soc. 2012; 134:13160–13163. [PubMed: 22852530]

(53). McGinnis JL, Dunkle JA, Cate JH, Weeks KM. The mechanisms of RNA SHAPE chemistry. J. Am. Chem. Soc. 2012; 134:6617–6624. [PubMed: 22475022]

(54). Lemay JF, Lafontaine DA. Core requirements of the adenine riboswitch aptamer for ligand binding. RNA. 2007; 13:339–350. [PubMed: 17200422]

(55). Dixon N, Duncan JN, Geerlings T, Dunstan MS, McCarthy JE, Leys D, Micklefield J. Reengineering orthogonally selective riboswitches. Proc. Natl. Acad. Sci. U.S.A. 2010; 107:2830–2835. [PubMed: 20133756]

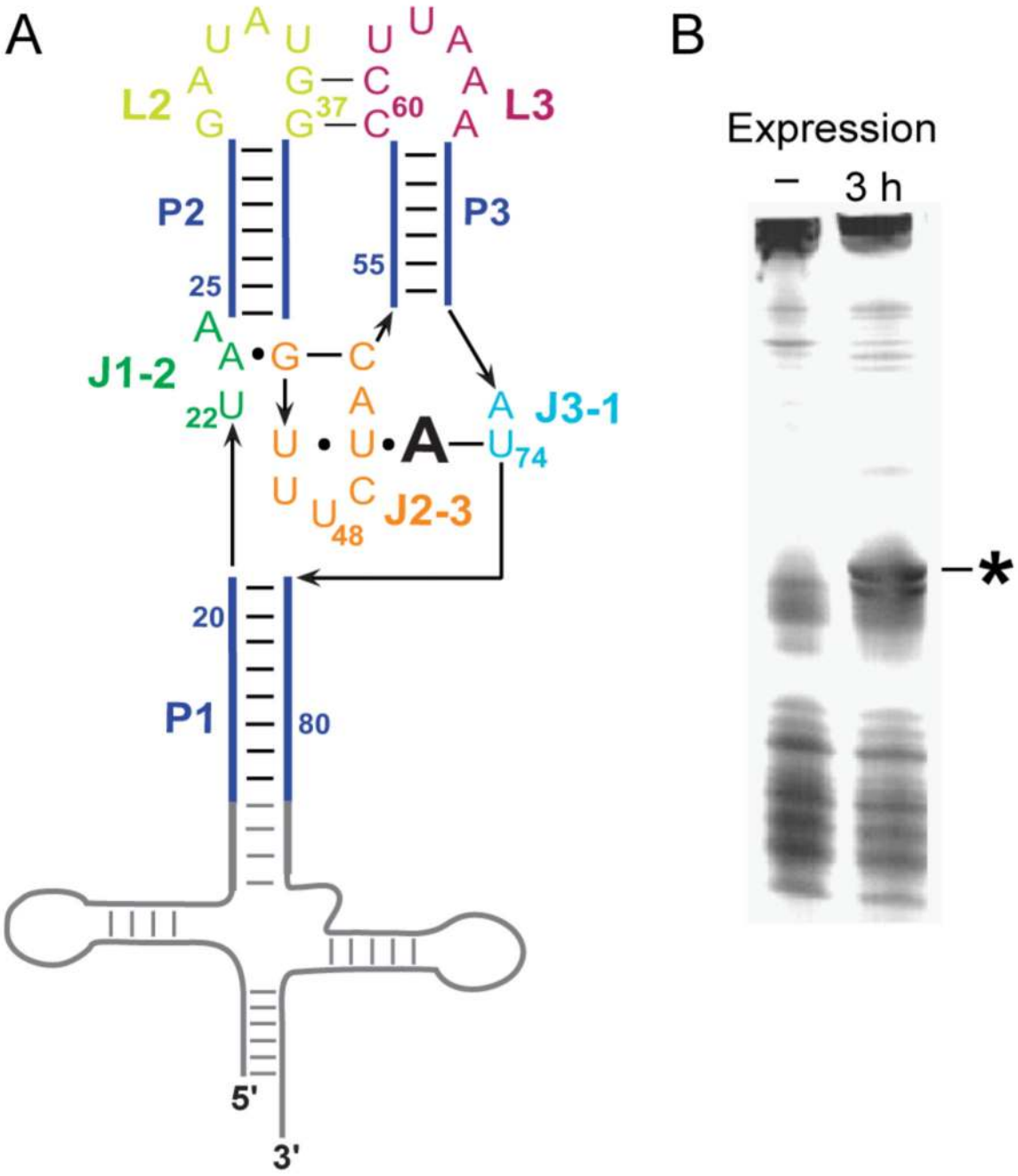


**Figure 1.**

Expression of the adenine aptamer domain in *E. coli*. (A) Structure of the aptamer-tRNA construct. The adenine ligand is shown as a large A. Numbering corresponds to the *add* aptamer domain.[32] (B) Total cellular RNA 3 h after inducing aptamer expression, visualized by denaturing polyacrylamide gel electrophoresis. The 143-nt aptamer-tRNA chimera product is marked with an asterisk.

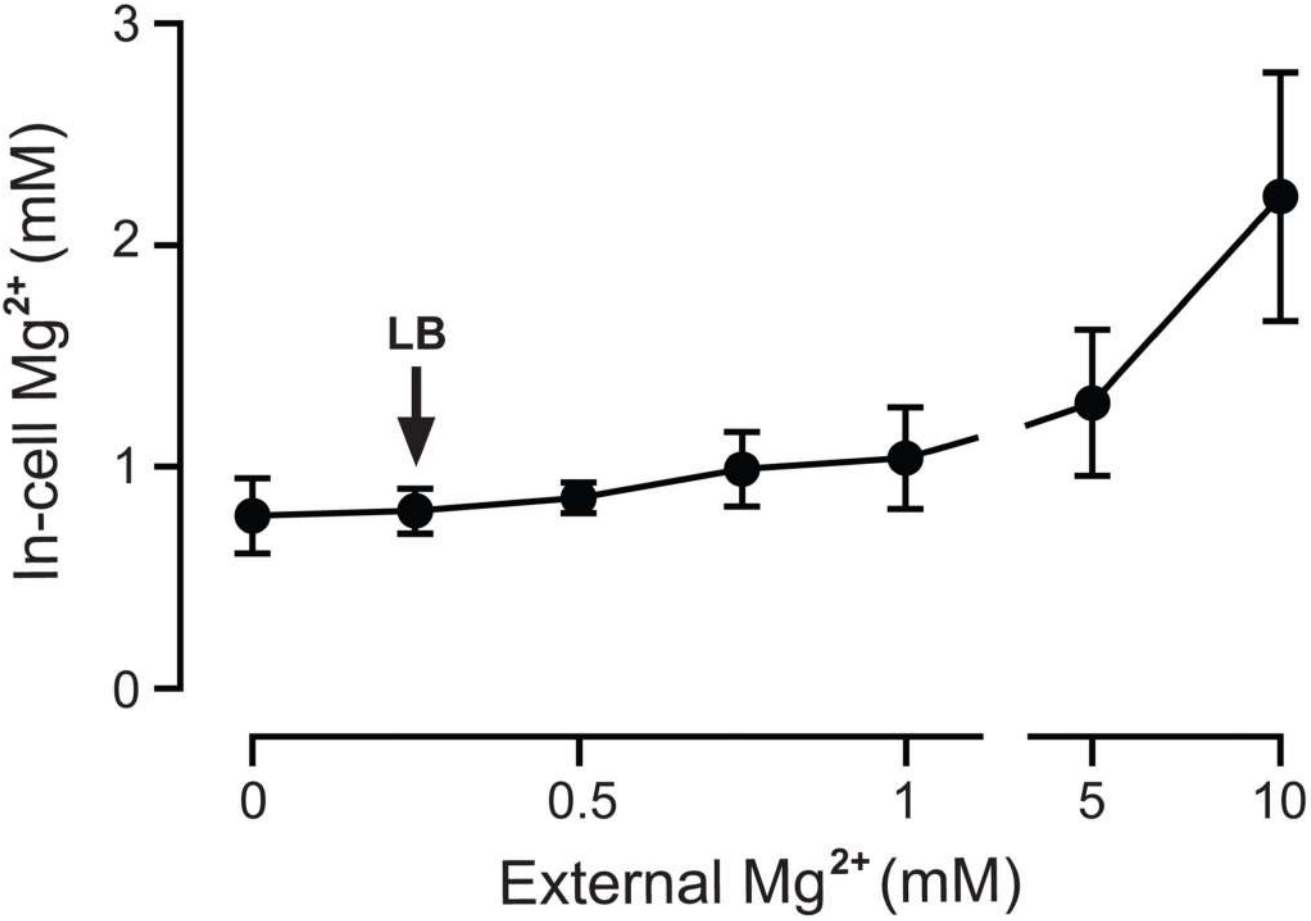


**Figure 2.**

Free $Mg^{2+}$ concentration in *E. coli* cells measured using the ion-selective fluorophore, mag-fura-2. The free concentration in cells at late-log phase is 0.8 ± 0.2 mM in standard LB media at 37 °C (arrow). The external concentration in standard LB media is 0.25 mM. Error bars show the standard deviation of the mean from three trials.

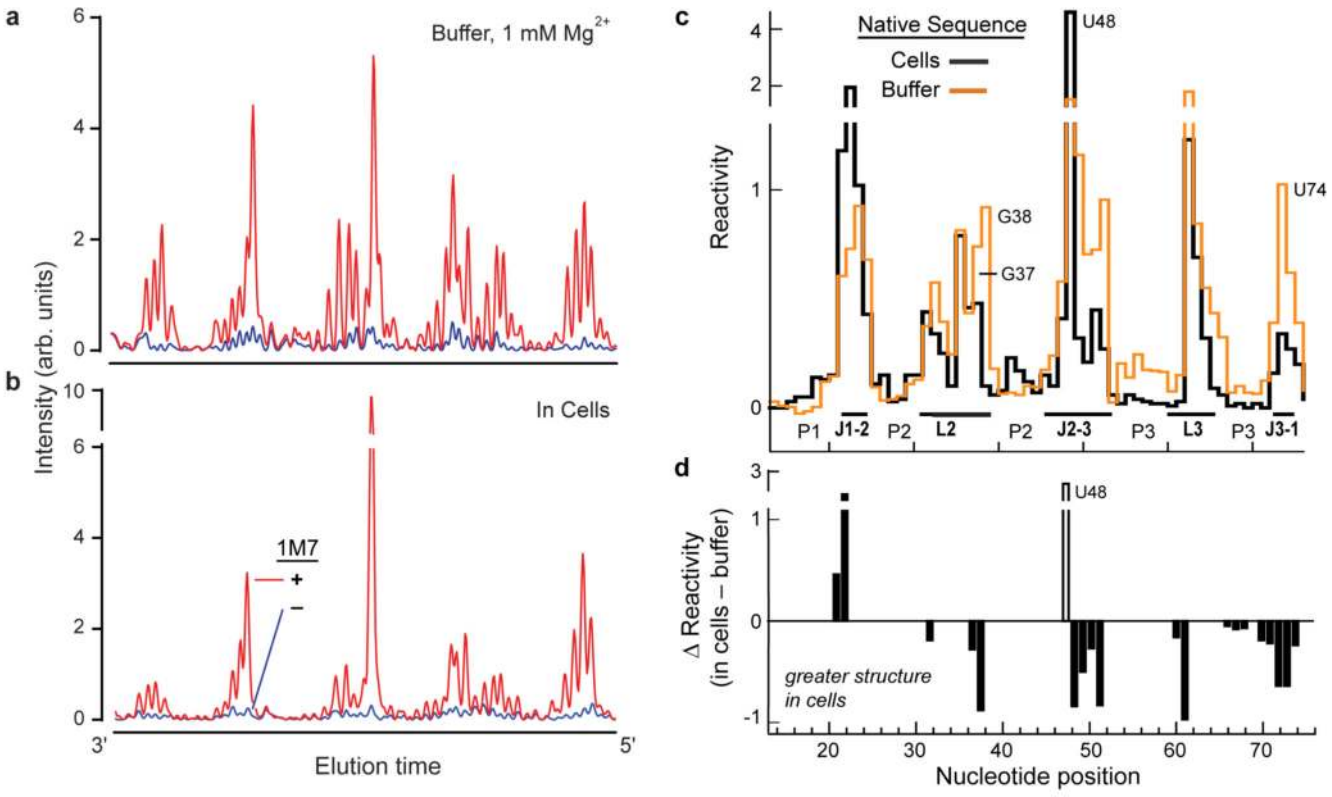


**Figure 3.**

In-cell SHAPE. Electropherograms showing SHAPE reactivity profiles for the native sequence adenine aptamer domain obtained (A) in buffer at a near-physiological $Mg^{2+}$ (1 mM) and (B) in cells. (C) Processed SHAPE reactivity profiles for the adenine aptamer domain in cells (black) and in buffer at 1 mM $Mg^{2+}$ (orange). (D) Difference plot comparing SHAPE reactivities in cells compared to buffer. Only statistically significant differences are shown (two-tailed Students t-test; $p < 0.02$, $n = 3$). Open box indicates that U48 is constrained in a rare hyper-reactive conformation (Figure S7 of Supporting Information); thus, a positive difference at this position reflects a higher level of structure in cells.

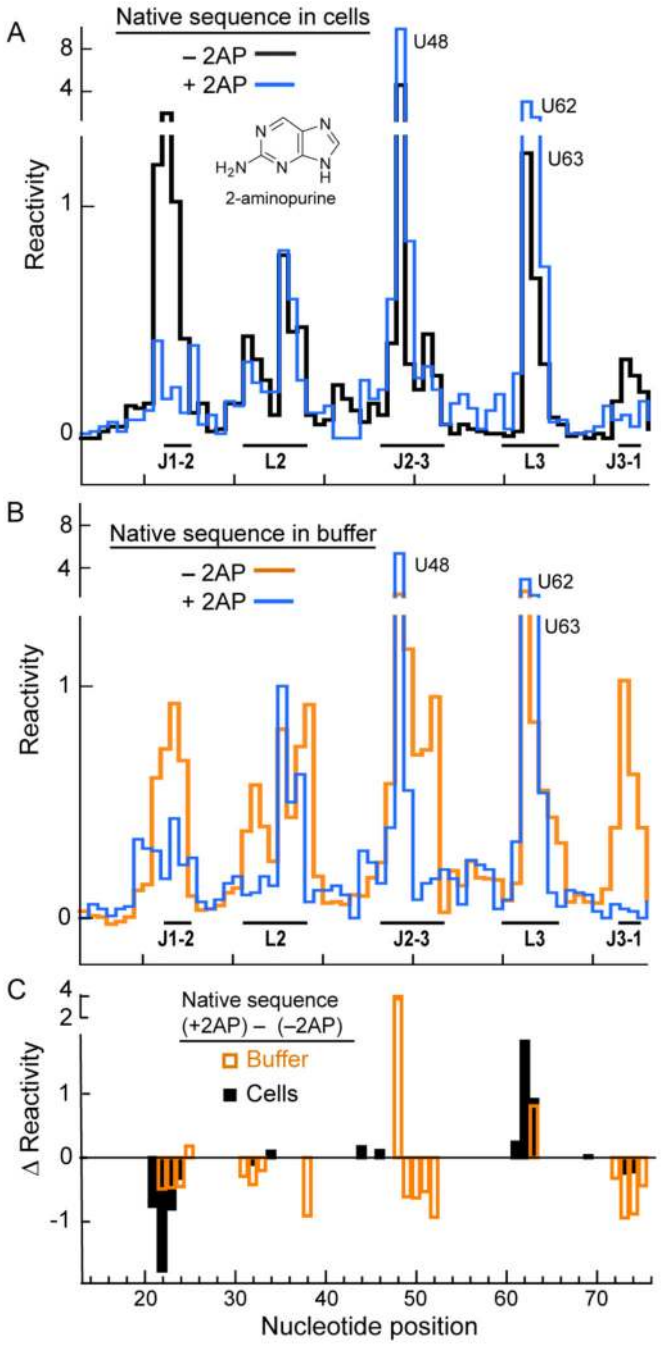


**Figure 4.**

Ligand binding by the native sequence adenine aptamer in (A) cells and (B) in buffer. When present, the 2AP ligand concentration was 1 mM. (C) Difference plot showing nucleotides with significant changes (two-tailed Students t-test; $p < 0.02$, $n = 3$) in reactivity upon ligand binding in-cells (black) and in buffer (orange).

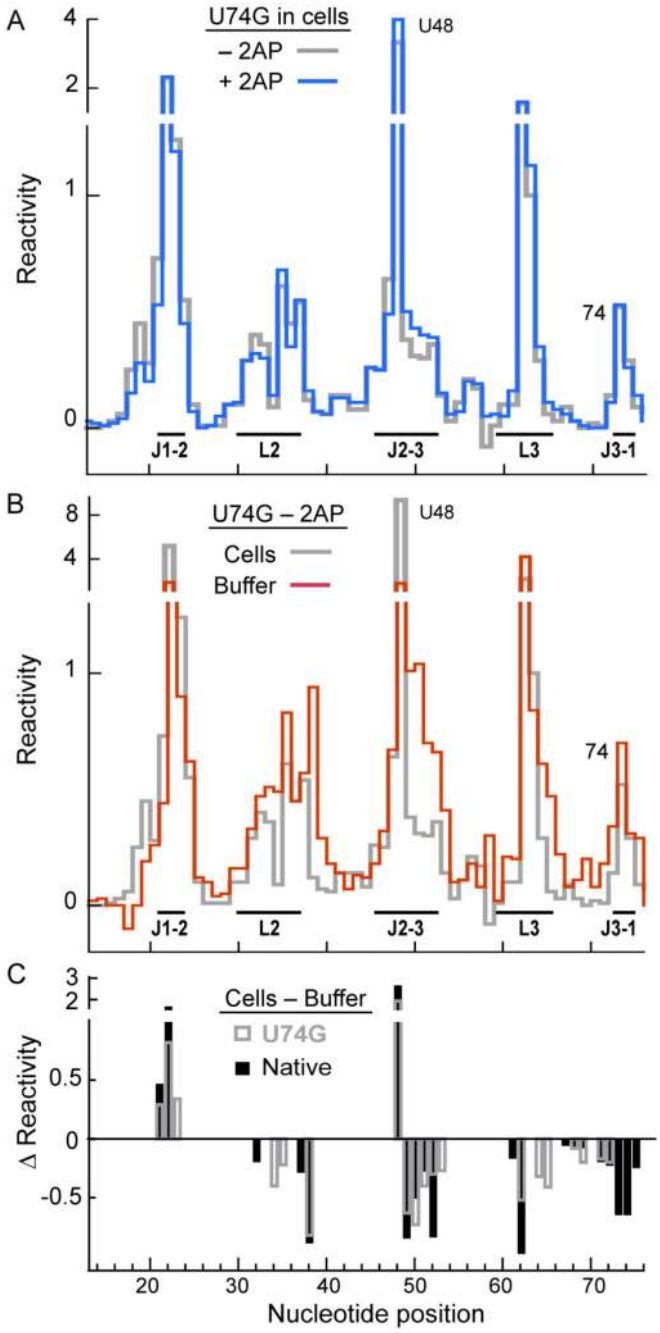


**Figure 5.**

SHAPE reactivity profiles for the U74G non-binding mutant (A) in the absence (gray) and presence (blue) of ligand in cells and (B) in the absence of ligand in cells (gray) and in buffer (red). (C) Significant reactivity differences in cells compared to buffer with 1 mM $Mg^{2+}$ for the wild-type (solid black bars) and U74G mutant (open gray bars) (two-tailed Students t-test; $p < 0.02$, n=3).

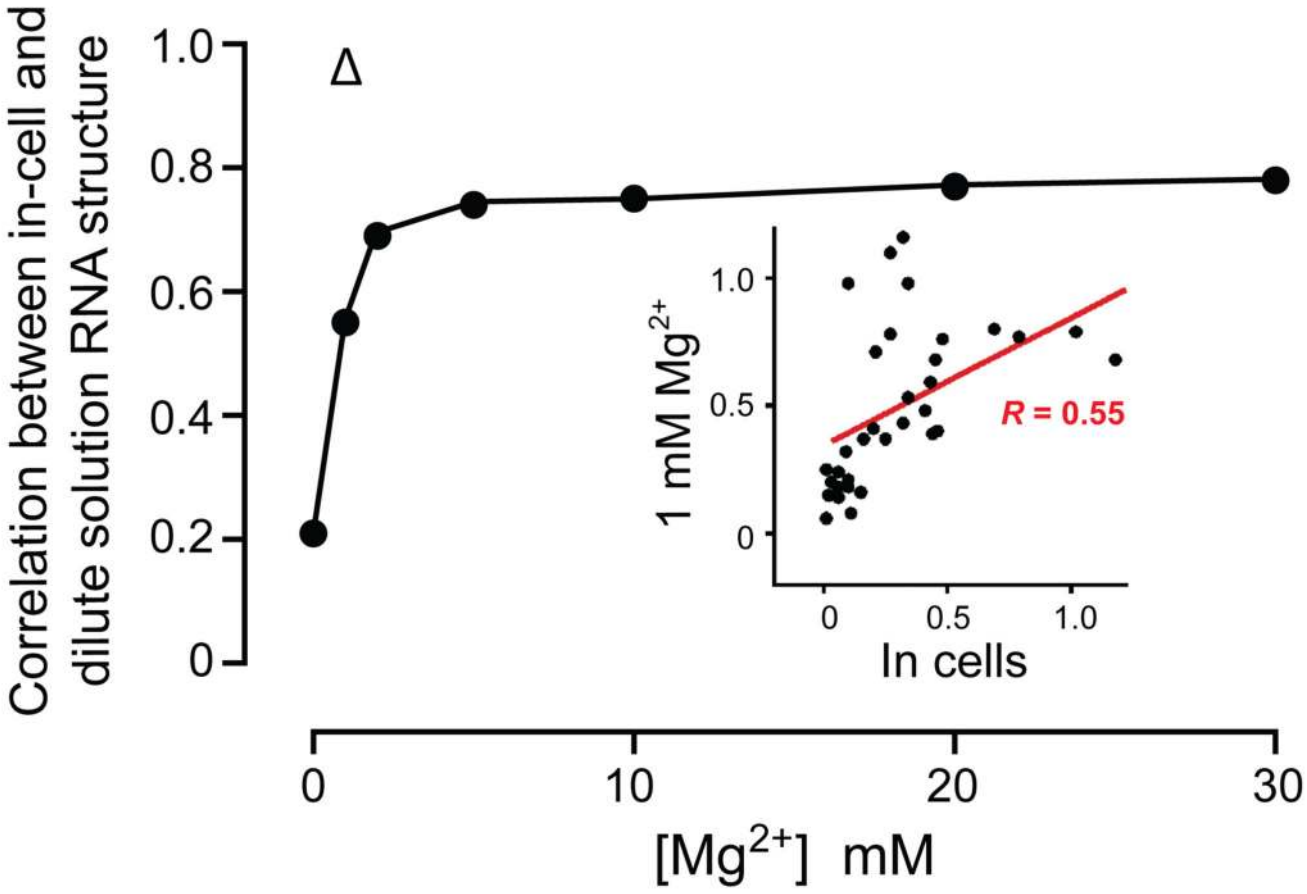


**Figure 6.**

Correlation between in-cell and *in vitro* SHAPE reactivities for the ligand-free aptamer domain as a function of $Mg^{2+}$ concentration. Data shown are from single-stranded and terminal base-paired nucleotides (A21-U25, U31-U39, A45-C54, G59-C67, and G72-U75) because these nucleotides show the largest structurally diagnostic changes. This correlation represents an upper limit. Inclusion of helix nucleotides, most of which have larger percent errors, results in an even poorer correlation (Figure S11 of Supporting Information). The open triangle represents the correlation between in cells and *in vitro* reactivities for the ligand-bound aptamer domain in 1 mM $Mg^{2+}$. *Inset*: *In vitro* reactivities at 1 mM $Mg^{2+}$ plotted against in-cell reactivities in the absence of ligand.

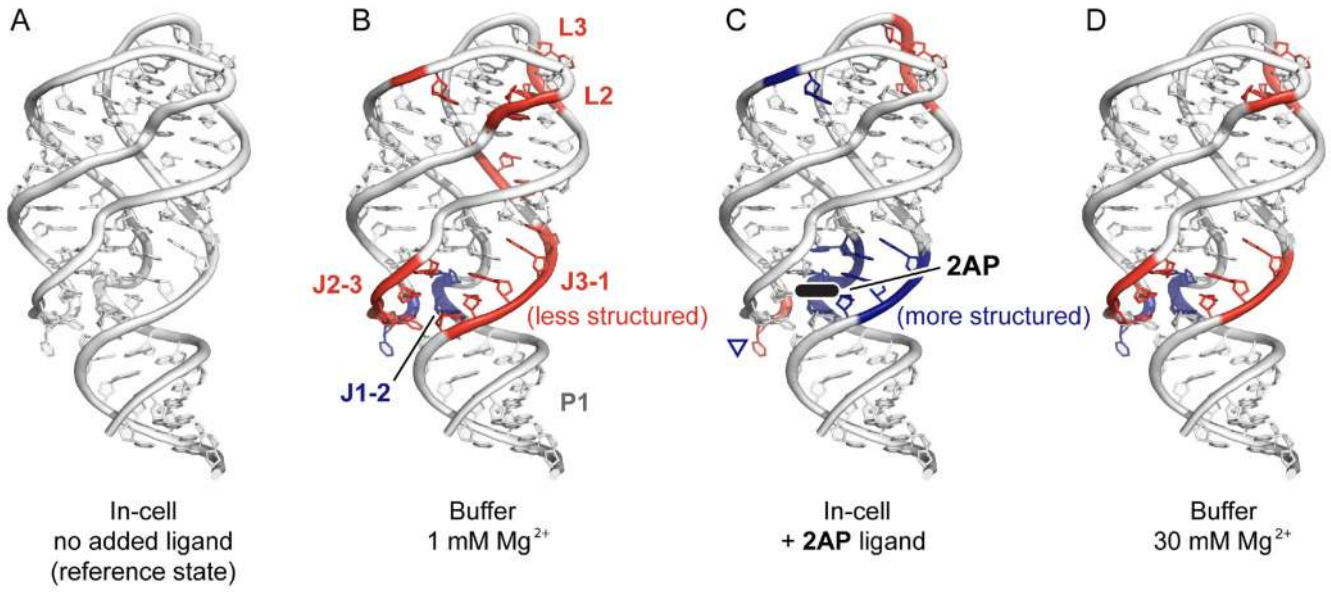


**Figure 7.**

Nucleotide-resolution effects of the intracellular environment on adenine riboswitch aptamer domain RNA structure superimposed on the accepted ligand-bound structure (PDB ID 1y26[32]) (A) The in-cell structure with no added ligand is defined as the reference state. Significant increases and decreases in nucleotide-resolution SHAPE reactivities relative to the in-cell RNA are emphasized in red and blue, respectively. Comparisons of the in-cell state with the aptamer RNA (B) in buffer at 1 mM $Mg^{2+}$, (C) in cells with added 2AP ligand, and (D) in buffer at 30 mM $Mg^{2+}$. The 2AP ligand, present in panel C, is shown in black. The inverted blue triangle in panel C indicates that U48 is constrained in a hyper-reactive conformation (Figure S7 of Supporting Information); thus, a higher (red) reactivity at this position reflects increased (blue) structure in cells.